RSC Advances

ROYAL SOCIETY OF CHEMISTRY

www.rsc.org/advances

Journal Name

RSCPublishing

ARTICLE

Effect of morphologies of CuS upon the photo-catalytic degradation of organic dyes

Cite this: DOI: 10.1039/xoxxoooooox

M. Tanveer[1], Chuanbao Cao[1], Imran Aslam[1], Zulfiqar Ali[1], Faryal Idrees[1], Muhammad Tahir[1], Waheed S. Khan[1], Faheem K. Butt[1] and Asif Mahmood[2]

Received ooth may 2014,
Accepted ooth may 2014

DOI: 10.1039/xoxxoooooox

www.rsc.org/

A variety of well defined, highly symmetric, super complex and hierarchical architectures of covellite copper sulfide have been successfully prepared by a simple solvothermal approach. The effect of various influencing parameters on the formation of CuS hierarchical architectures has been precisely investigated and a possible formation mechanism has been elucidated. The exposure time has been found to be a critical factor in controlling the CuS architecture and highly complex structures were obtained under elongated reaction times. The "as synthesized" architectures exhibited excellent photocatalytic activity in visible region for catalysis of individual dye (methylene blue and rhodamine B) and their mixed solutions in presence of H_2O_2. The efficient photocatalytic activity can be attributed to carefully controlled hierarchical CuS structures. Overall, this study is of great importance in "bottom-up" assembly of copper sulfide nanoplates to obtain highly complex structures which offer a good opportunity to understand the fundamental significance of atypical structures for their potential applications.

Introduction

Morphological and structural tailoring of nano/micro crystals has been emerged as an exciting challenge for current material synthesis due to the special shape and structure dependent unusual effects, which would develop their significant scientific values and widespread, versatile potential applications.[1] The hollow three-dimensional (3D) superstructures as one type of prospective structures with low density, large surface area, good conductivity and permeability, for charge and mass (gas) transport, have drawn utmost research interest because of their potential applications in sensors, catalysts, drug-delivery carriers, lithium ion batteries, etc.[2–7] Moreover the hierarchical structures not only provide a specific surface area but also a more dispersed active site for the catalyst. This structure is found much stable under any atmospheric environmental conditions; thus, catalysts with such structure can be maintained at a highly efficient catalytic level after several repeated catalytic reactions. In particular, the three-dimensional (3D) hierarchical architectures assembled by nanostructured building blocks such as nanorods, nanoribbons, nanosheets and nanoparticles have been well investigated for their much improved properties originating from their building blocks and other functional applications. These distinguishing features could be expected to be more advantageous rather than those of the powder samples, matching well with the principles of a highly efficient catalyst designs.[8-11] The hollow and 3D superstructures with different building blocks can be successfully synthesized by precisely controlling the nucleation and growth via a ''bottom–up'' self-assembly route. Many recent efforts have been employed to the synthesis of hollow architectures; however, most of the synthesized hollow architectures are spherical shaped and having polycrystalline shells.[2] As a non-stoichiometric p-type semiconductor (direct band gap 1.2–2.0eV) with unique optical, electric and thermal properties,[2–4] copper sulfide is a promising material with applications in solar cells, optical filters, nanoswitches, thermoelectric and photoelectric transformers, superconductors, gas sensors and lithium-ion batteries.[2–4, 12] For the above applications, a microstructure tailoring which determines the surface atomic arrangement and surface energy is of great importance. So far, non-spherical copper sulfide micro- and nanocages with single-crystalline shells (such as cubes, octahedra and 18- facet polyhedra) have been artificially synthesized by using cuprous oxide (Cu_2O) crystals as sacrificial templates.[2–4] Much attention has been recently developed towards Cu_2O-templated growth of various copper sulfide cages, the general approach for preparation of hollow and complex structures for versatile applications has involved the significance use of various removable or the sacrificial templates, including hard ones such as mono disperse silica polymer latex spheres as well as soft templates.[13] However, the hollow and complex structures prepared from hard templating routes mostly suffer from disadvantages related to their high cost and tedious synthetic procedures. However, there have been fewer reports about the controlled and template free synthesis of diverse morphologies displaying more complexity with a highly geometrical shape. Recently, a novel morphology in the form of ball-flowers has been reported through a well controlled template free hydrothermal pathway, but still the control over the architectural synthesis has been achieved with the assistance of a surfactant (Polyvinylpyrrolidone, PVP).[14] These ball-flowers architectures have been employed to ascertain the photo-degradation of RhB aqueous solution under Ultraviolet light. Herein we report the synthesis of well defined hierarchical architectures of CuS with good control over size and shape by template and surfactant free

synthetic approach starting from irregularly joined nanoplates, Single Wall Cuboctahedrons (SWCOs), Double Wall Cuboctahedrons (DWCOs), Multi Wall Cuboctahedrons (MWCOs) up to Super Complex Cuboctahedrons (SCCOs) with extraordinary controlling capability through simple variation of certain reaction parameters. The "as prepared" architectures provide better crystallographic design enriching family of copper sulfide nanostructures. Moreover the structural, optical properties and natural light driven versatile photocatalytic activities of these "as prepared" unusual and complex architectures has been ascertained and a precise comparison has been carried out. The synthesized materials show high degradation of dye solutions (MB, RhB, MB+RhB) with repeatedly reusable capability under irradiation of natural light, which can be successfully applied for decomposition of industrial pollutants at pilot scale.

Experimental

Sample preparation

In a typical solvothermal synthesis, 1mmol of $Cu(NO_3)_2.3H_2O$ were dissolved in 40ml of ethylene glycol (EG) to form a clear blue solution, then after complete dissolution 2mmol finely dispersed sulfur powder was added to the above solution under vigorous stirring for 30 minutes. Afterward the solution was transferred into a 50ml capacity Teflon lined stainless steel autoclave. The autoclave was sealed and maintained at 180°C for 24h, the obtained black solid products were collected by centrifuging the mixture; these solid products were then washed with distilled water, absolute ethanol and acetone several times each and dried in a vacuum at 80°C for 8h before further characterizations. The same typical experiment was repeated several times for different reaction durations (4h, 8h, 12h and 18h), at different temperatures (140 °C, 160 °C, 180 °C and 200 °C), in the presence of different solvents and variety of Cu, sulfur sources to obtain a thorough understanding of growth mechanism and effects of different parameters upon the architectured synthesis of unusual morphologies of CuS. In analogy the products obtained under typical experimental condition at 8, 12, 18, 24h, will be denoted hereafter as single wall cuboctahedrons (SWCO), double wall cuboctahedrons (DWCO), multiwall cuboctahedrons (MWCO) and super complex cuboctahedrons (SCCO), respectively.

Chracterization

X-ray diffraction (XRD) patterns of the products were recorded on a (XRD, PhilipsX'pert Pro X-ray diffractometer) equipped with 1.5406Å Cu Kα radiations in the 2θ range of 20°-80°. Whereas, the morphological characterizations were ascertained by scanning electron microscopy (SEM, Hitachi TM-1000) and energy dispersive x-ray spectroscopy (EDS) was used to determine the chemical composition of the products. The X-ray photoelectron spectroscopy (XPS) spectra were recorded on a Rigaku XPS 7000 spectrometer using non monochromatic Mg K (alpha) (1253.6eV) at a source of 200W, chamber pressures during the measurement was about 10^{-7}Pa. The binding energies were referred to the adventitious C 1s peak at 284.6eV. Transmission electron microscopy (TEM) photographs and electron diffraction (ED) were performed on a Philips CM 200 (200 KV) transmission electron microscope. Optical properties of the samples were studied at room temperature using Ultraviolet–visible–near infrared (UV–vis–NIR) transmittance spectrophotometer (U-4100) and Photoluminescence properties were visualized by F-4500 Fluorescence Spectrophotometer.

Photo-catalytic activity evaluation

MB and RhB and mixture of these dyes have been selected for evaluation of catalytic activity. All experiments were carried out in the presence of natural light and H_2O_2 was added to provide localized hydroxyl ions which trigger the catalytic process. In a typical experiment, the solutions were prepared by taking 2.8mL ($400mgL^{-1}$) of the MB and RhB separately and adding 2mL H_2O_2 (30%, w/w) in each of the dye solution followed by dilution of the solutions up to 100mL. Similary, mixed solution of the two dyes (MB+RhB) was prepared and volume was raised to 100mL. Then 20mg of the as-prepared CuS hierarchical SCCO was added into the solution to form the aqueous dispersion. The solution was magnetically stirred in the dark for 30min to ensure the establishment of an adsorption–desorption equilibrium before illumination. The dye dispersions were then subjected to irradiation of natural light with continuous stirring. Samples were taken after specific time intervals followed by centrifugation prior to UV-Vis analysis for reaction monitoring. The UV-Vis spectra were obtained by using UV spectrophotometer (Hitachi U-4100) and the degradation was visualized following the absorption peaks at 604nm for MB and 553nm for RhB. The photocatalytic properties of other synthesized materials (DWCO, SWCO) as well as dense commercial CuS powder (9.04 m^2g^{-1}; surface area) have also been studied for comparative analysis. After complete degradation, catalysts (CuS) were obtained for reuse by centrifugation. The catalysts were used for 6 cycles successively to completely evaluate the reusability of the catalysts and their applications in potential water treatment applications. The catalytic decolorization of the dye solution is a pseudo-first-order reaction and the degradation rate is calculated by the following formula.[15]

$$\text{Degradation (\%)} = (1 - C_t/C_o) \times 100\% \quad (1)$$

Where, C_o and C_t represent the initial concentration of the dye and the concentration at time t, respectively.

Results and Discussion

Structural and morphological characterizations

The phase purity and crystallinity of the as prepared CuS SCCO was characterized employing XRD technique. As shown in Figure 1 display the XRD pattern of as synthesized SCCO, all the diffraction peaks have been indexed as hexagonal covellite-type CuS with the calculated cell parameters a= 3.7920Å, b= 3.7920Å c= 16.3440Å which is in good agreement with the literature values (covellite, syn, JCPDS No: 00-006-0464). The XRD pattern confirmed that the product is devoid of any detectable impurities. The energy-dispersive spectra (EDS) analysis of the as prepared product shown in Figure 3d demonstrates that the chemical components only consist of Cu and S elements with an atomic ratio (Cu: S= 1:1), in agreement with the above XRD result.

Figure 2 depicts X-ray photoelectron spectroscopy (XPS) analysis of SCCO carried to ascertain the chemical composition, purity of the prepared sample and to identify the chemical status of Cu element in the sample. Figure 2a exhibits the XPS survey spectrum, the presence of Cu peaks of Cu 2p, S 2p, O 1s, and C 1s can be clearly observed. The weak peaks of O and C come from H_2O, O_2, and CO_2 adsorbed on the surface of the sample and adventitious hydrocarbon from XPS instrument itself, respectively.[16]

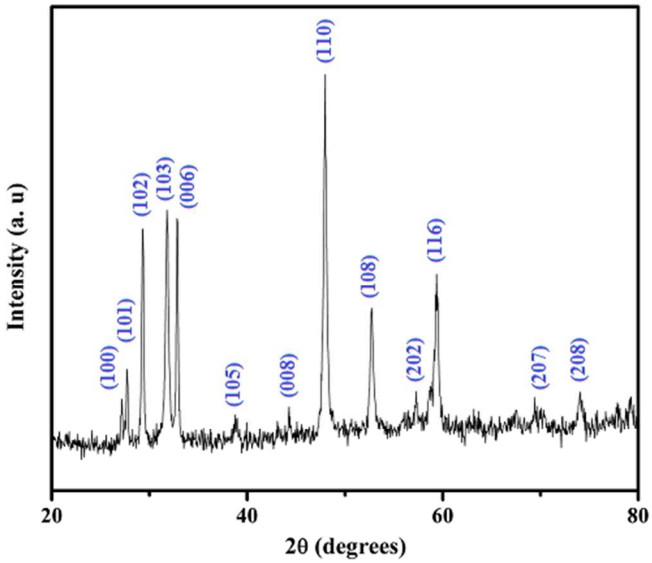

Figure 1. XRD spectrum of CuS SCCO.

Figure 2b is representing high resolution spectrum of Cu 2p and it is obvious that the presence of two strong peaks separated by 20.0eV at 932.3eV and 952.3eV for Cu 2p3/2 and Cu 2p1/2, respectively, are essentially identical binding energies for the Cu 2p orbital in accord with Cu(II).[16]

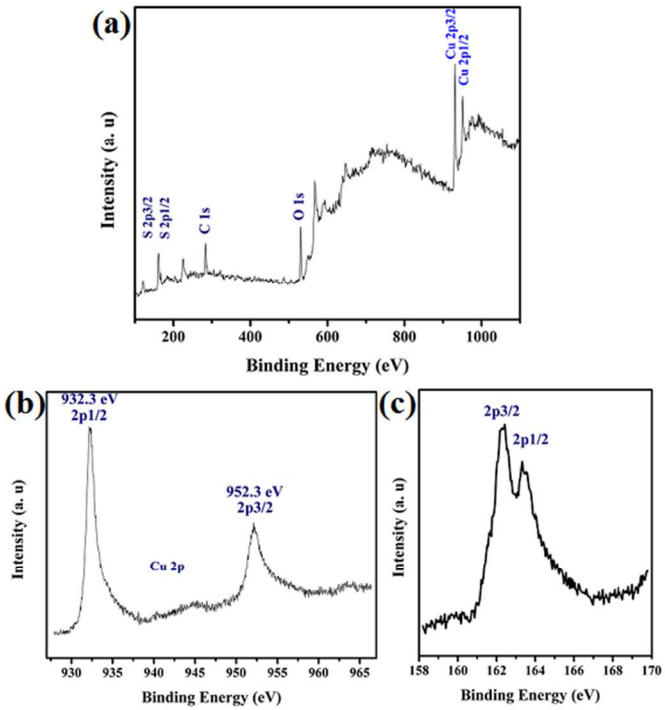

Figure 2. XPS spectrum of the as-synthesized CuS SCCO (a) XPS spectra of survey of the as-synthesized CuS SCCO, (b) XPS spectra of close-up survey in the Cu 2p region, (c) XPS spectra of close-up survey in the S 2p region.

In addition, a small chemical shift about (0.3eV) has occurred compared to the elemental copper. Meanwhile, two shakeup satellite lines at 943.0 and 963.6eV are observed, which are the characteristic of materials having d(9) configuration in the ground state, that is, Cu(II),[17] indicating the paramagnetic chemical state of Cu^{2+} Furthermore, symmetrical shapes of the two Cu 2p XPS peaks also imply the presence of pure phase CuS. In Figure 2c, the high resolution survey at the S 2p region shows the presence of two peaks at 162.4eV and 163.3eV, all these peak positions are well matched with literature.[18] The Cu/S ratio was calculated from the peak areas of Cu and S-cores, the value was found to be 1.01 that is closely matched with the Cu/S value estimated from EDS analysis.

Figure 3 is the typical SEM images of the as prepared hierarchical SCCO with nanoplates building blocks at different magnifications. From the low-magnification SEM result (Figure 3a), it is obvious that CuS SCCO have high yield, the excellent hierarchical architectures with amazingly well defined and interconnected unique nanoplates as building blocks at large scale. The images in Figure 3a, b clearly indicate shape and size consistency and high yield of the product, all of the SCCO are well defined, quite consistent and separately displaced. In the corresponding magnified image in Figure 3c, it can also be ascertained the SCCO are architectured identically with nanoplates, much complex and well interconnected. Moreover, there are a lot of cavities among the individually and hierarchically connected nanoplates within each entirely isolated SCCO microstructure. The hierarchically connected nanoplates are few nanometers in thickness, connected identically to create deep and capacious pores with each unusual and complex mircrostucture of SCCO.

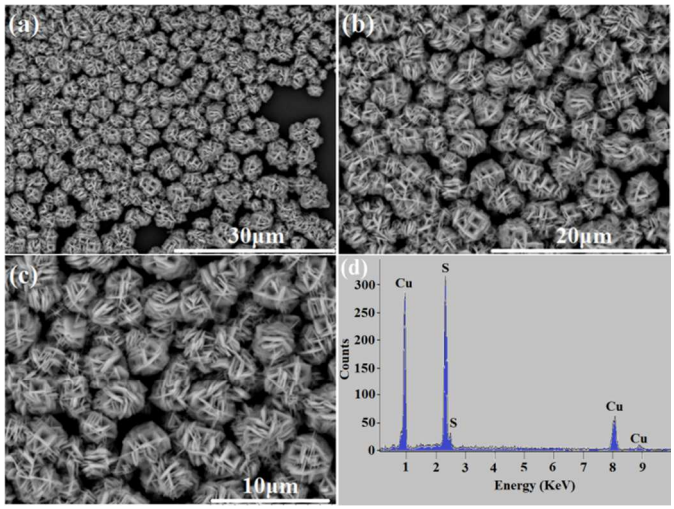

Figure 3. (a, b, c) SEM images of CuS SCCO, (d) EDS spectrum of as prepared supreme hierarchical SCCO.

Further detailed structural characterizations of as prepared CuS SCCO were performed by TEM and HRTEM. Figure 4a displays the TEM image of the as prepared SCCO the strong contrast between the dark edge and pale portions is the obvious evidence of cavities within the entire hierarchical existence as synthesized architectures. From the high magnification TEM image of SCCO (inset of Figure 4a), it is clear that each hierarchical structure is entirely composed of nanoplates having thickness in a few nanometers and joined in a well defined manners.

The HRTEM image conducted on the scattered nanoplates is given in Figure 4b. From the top view the regular spacing of the clear lattice planes is calculated to be 0.312 nm, match well with the interlayer spacing's of (102) crystallographic plane of hexagonal CuS.[32]

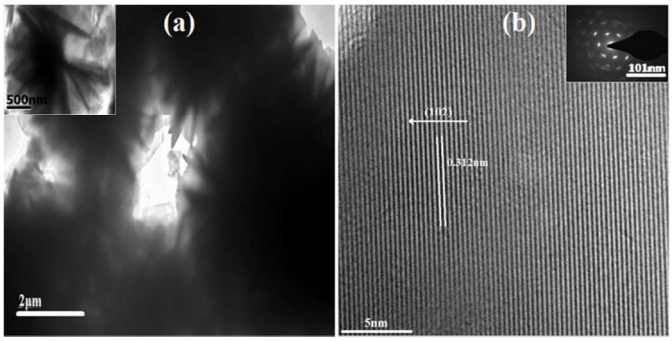

Figure 4. (a) TEM image of CuS SCCO, (inset is the high magnification TEM image of CuS SCCO) (b) HRTEM image of CuS SCCO, (inset is the SAED pattern of CuS SCCO).

Moreover, the scattered area electron diffraction (SAED) pattern (Figure 4b, inset) was recorded for to further investigate the crystallographic features of the as prepared product, which displays clear image of lattice fringes well-matched with XRD results, indicating good crystalline and hexagonal crystal structure. The well-defined spots in the SAED spectra illustrate the perfect growth of single crystals of CuS, confirming the SCCO to be having same crystallographic orientation along the nanoplates axis as a perfect single crystal. The formation of SCCO started from a nucleus, as soon as the reaction parameters reached the optimized condition. These nuclei started growth in specific directions to form nanoplates which then join together to form highly connected structures by self assembly involving bending and aggregation.[33]

Effect of reaction duration and formation of SCCO of CuS

The growth of SCCO was further studied with time dependent synthesis experiments while all other parameters were kept constant as that of typical experimental process. It is observed that exposure time plays critical role in controlled synthesis of CuS structures. At lower exposure times (4h), homogenous self assembled CuS sulfide nanoplates were obtained (Figure 4a) along with random aggregations which show incompletion of morphological evolution process under these conditions. An increase in reaction duration up to 8h provided well defined SWCO as shown in Figure 4b. The structures obtained under current conditions consist of four identical hexagonal plates and the overall structure shares 24 identical edges in a dymaxion way, each cuboctahedron with 14 faces can be simplified as having a composition of six squares and eight triangles. A similar architectural performance for the first time was performed earlier, employing the same reaction media along with the same procedure at 160°C for 24h.[12] Herein, in our synthetic process, in order to observe the post synthesis of this morphology, for to obtain the more complex hierarchical architectures, the reaction was further prolonged to 12h. Upon further increase in reaction duration (12h), the nanoplates self assembled to form double wall cuboctahedrons (DWCO) with hollow cores as demonstrated in Figure 4c. At the elongated reaction time of 18h, multi-nanoplates were assembled into hierarchical structure, and the typical hierarchical multiwall cuboctahedrons (MWCO) were formed (Figure 4d). It is quite clear that further increase in reaction time increased complexity of the formed structure as demonstrated by the products synthesized after 24h of exposure time (Figure 3) and extremely complex morphology is observed. The diffraction spectrum of these CuS structures synthesized after different exposure times suggest no major phase difference. All the products are composed of rather same phase of CuS with XRD spectra corresponding to hexagonal CuS structure (JCPDS Card No. 06-0646) as shown in Figure S1. The slight difference in relative intensity at different exposure times could arise due to preferential growth in specific directions. The growth mechanism of CuS structures has also been proposed in the light of the above results. The metal salt source provides Cu^{2+} while EG provides reducing environment and sulfur is also present in liquid form in reaction chamber at high temperature.

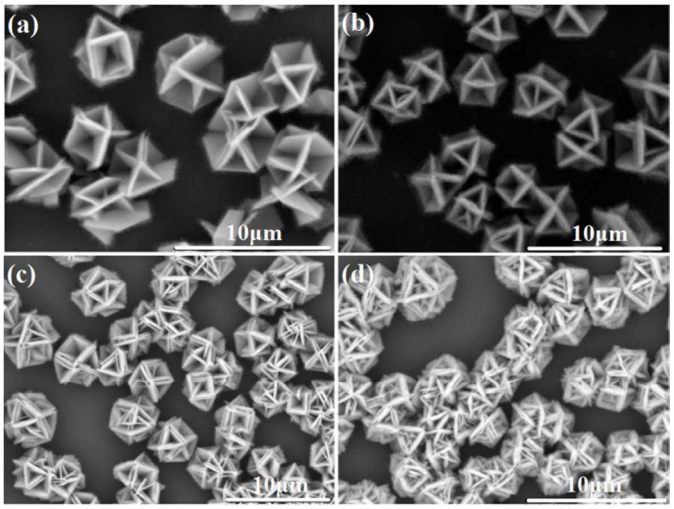

Figure 5. SEM images of the as prepared products at different reaction durations, under the same typical experimental conditions at 180°C (a) 4h, (b) 8h(SWCO), (c) 12h(DWCO), (d) 18h(MWCO).

In our system EG undergo dehydration[21] forming acetaldehyde as shown in following reaction.

$$2HOCH_2CH_2OH \xrightarrow{-2H_2O} 2CH_3CHO \quad (1)$$

$$2CH_3CHO \rightarrow 2H_3CCOCOCH_3 + 2H \quad (2)$$

$$S + 2H \rightarrow H_2S \quad (3)$$

At high temperature, acetaldehyde provides hydrogen acting as reducing agent (eq. 2). S^{2-} ions are then formed through the reduction of element S by H atoms, as shown in eq. (3) and Cu^{2+} ions react with S^{2-} ions, which precipitate to become the CuS nuclei and quickly grew into the primary particles. Actually sulfur melts at high temperatures forming small droplets in the solvent which act as microreactors for the growth of CuS thus providing sound base for directional growth. The heating process makes uniform S sphere droplets and reactive H_2S, simultaneously. The whole evolution process is illustrated schematically in Figure 6. On the whole, a two-tiered organizing scheme for construction of hierarchical CuS nanostructures has been elucidated: (1) nanoscale formation of building units via oriented aggregation, i.e. nanoplates; (2) macroscopic organization of these building units into hierarchical CuS nanostructures. So, exposure time and temperature appear to be most critical factors in designing defined structures of CuS. So, the growth process follows a two step process involving aggregation and crystallization. The reaction leads to formation of nanoplates which join together through several types of attractive forces such as hydrogen bonding, crystal-face attraction, Vander Waals forces or electrostatic forces.[22, 23] Optimizing conditions give well defined SWCO, DWCO and MWCO along with hierarchical SCCO. To explore the influence of various copper, sulfur sources (Figure S2) and a variety of solvents (Figure S3) on the formation of unusual morphologies of CuS SCCO, a series of comparative experiments were performed under similar typical experimental conditions. Overall among the comparative experiments, neither the use of other

Cu^{2+} sources with different anions nor the use of other sulfur sources or any other solvent except ethylene glycol could lead to formation of amazingly well-defined hierarchical complex caved cuboctahedrons.

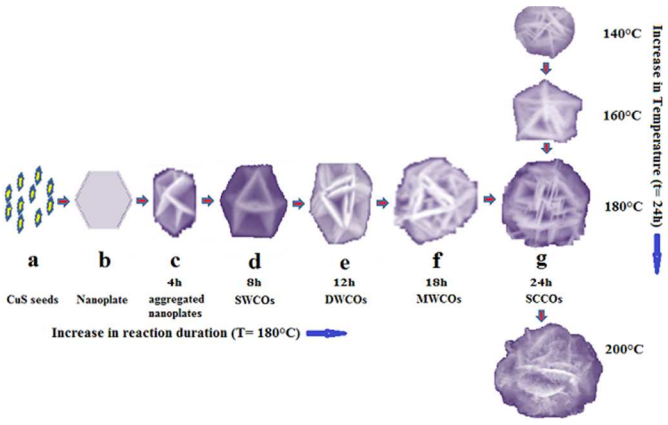

Figure 6. Growth mechanism of CuS SCCO.

Moreover the reaction temperature (Figure S4) also highly affected the morphology the CuS nanomaterials. At lower temperature the nano architectures are made up of densely packed nanoplates with very thin thickness, and aggregated irregularly. Whereas, at intermediate temperaturs all hierarchical microstructures consist of sparsely packed nanoplates and well interconnected with a definite shape and size in quite regular manners. At much higher reaction temperature beyond a certain limit the as prepared hierarchical architectures appeared to be distorted.

Optical properties and BET surface area

The UV–vis absorption spectra of unusual and complex architectures of CuS, such as, SWCO, DWCO, MWCO and SCCO are shown in Figure 7a. All of the absorption spectra exhibit a characteristic covellite CuS like absorption band in the near-IR region,[25-26] due to inter band transitions (absorptions) from valence states to the unoccupied states.[27] Compared with bulk covellite CuS[28], SWCO, DWCO, and MWCO, the as prepared super hierarchical SCCO exhibits a large and distinct blue-shift, which is possibly attributed to the special morphological effect of very thin nanoplates intersected CuS SCCO. The small absorption differences between the absorption peaks in spectra of as prepared unusual morphologies is possibly due to the size and morphology differences of as prepared CuS products. Moreover, according to the equation $\alpha E_p = K(E_p - E_g)^{1/2}$, a plot of $(\alpha E_p)^2$ Vs E_p based on the direct transition of as prepared products is shown in the inset of Figure 7a, the extrapolated value of E_p at R= 0 gives absorption edge energies correspondence to *E*g = 1.70, 1.86, 1.90, 1.96eV for the as prepared products; SWCO, DWCO, MWCO and SCCO, respectively. The larger band gap of supreme hierarchical SCCO has been visualized in comparison with SWCO, DWCO and MWCO.

Figure 7b shows the room temperature PL spectra of unusual and complex architectures of CuS, such as, SWCO, DWCO, MWCO, SCCO, respectively. All of these emission spectra were obtained with the excitation wavelength of 370nm. The as prepared CuS architectures exhibit similar emission features, including a strong and weak emission peaks. The emissions spectra of SWCO, DWCO and MWCO show a strong emission peaks centered at 492nm, 468nm, 455nm, several shoulder peaks, respectively. Whereas, the SCCO show a blue shift in emission and strong emission peak of higher intensity centered at 410nm and very small shoulder peaks compared to other as prepared products, indicating much better, highly crystalline and good optical feature of the as prepared SCCO.

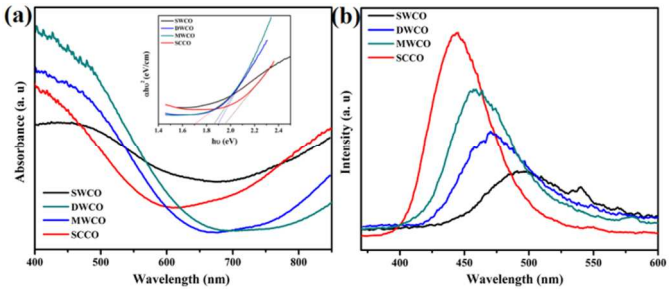

Figure 7. (a) UV-visible absorption spectrum, Band gap energy (inset) of as prepared CuS complex architectures, (b) PL spectrum of as-prepared as prepared CuS complex architectures.

Although Qin et al.[29] reported that there was no emission peak for CuS in the range of 400–800nm, our result is very consistent with the PL result reported by Ou et al.[30] and Kalyanikutty et al.[31] The size and morphology of the different CuS products may be responsible for the shift of blue and green emission peaks in spectra of SWCO, DWCO and MWCO, and the possibility of improvement in PL intensity due to higher crystallinity of SCCO cannot be ruled out. However, the origin of the observed optical properties is still far from well-understood, and more detailed investigations are needed.

The Brunauer–Emmett–Teller (BET) specific surface area of synthesized CuS products was investigated by nitrogen adsorption-desorption measurements. Figure S5 shows the nitrogen adsorption-desorption isotherms of as prepared CuS products. All the isotherms display a typical type IV curve with a hysteresis loop at relative pressure (P/P_0) between 0.0 and 1.0. The BET surface areas of the CuS SCCO, DWCO and SWCO were measured to be 41, 24.0 and 16 $m^2\ g^{-1}$, respectively and quite higher than the surface area of commercially available dense CuS powder (9.04 m^2g^{-1}). All the as synthesized hierarchical architectures due to cavities within the intersected nanoplates building blocks possess a mesoporous structure as evidenced by the nitrogen sorption. The BET surface area of SCCO has been found to be higher than the other as mentioned CuS products and commercial CuS. Moreover the supreme and complex architectures of CuS SCCO appeared to be having double pore size (inset, Figure S5). The unique double pore structures along with considerable high surface area makes a photo-catalyst promising candidate as a catalyst for the degradation of highly concentrated dye pollutions in wastewater along with excellent reusability.

Photo-catalytic properties

Figure S6 displays the adsorption and photo degradation curves of an aqueous solution of MB photo degraded by the CuS photo catalysts with different morphologies SCCO, DWCO, SWCO and commercially available CuS powder in the presence of hydrogen peroxide. The characteristic absorption peak at 604nm of MB was used as a monitored parameter during the photo-catalytic degradation process. H_2O_2 yielded highly reactive hydroxyl radicals that oxidize MB into smaller molecules such as CO_2, H_2O, etc. The catalytic property of CuS was found closely dependent to the amount of hydroxyl radicals; the assistance of H_2O_2 can be in favor of the bleaching of MB.[32–33] The H_2O_2 alone was found incapable to the degradation of dye solutions without the assistance of the catalyst (Figure S6a). Moreover, it is also observed that CuS catalyst in the absence of H_2O_2 is not capable to degrade the MB (Figure S6b). So the presence of H_2O_2 appeared to be necessary and crucial to assist

the catalytic activity of the CuS. Figure S6f shows the degradation of MB solution in the presence of H_2O_2 and as prepared CuS SCCO. The intensity of the absorption MB decreased rapidly with the extended exposure time. The degradation of aqueous MB solution in the presence of SCCO assisted by H_2O_2 was observed to be 35.7%, 61%, 75.5%, 86% and 96% after 10, 20, 30, 40 and 50min respectively (Figure 8a; Panel A) and maintained at a relatively stable level after this irradiation time. The DWCO as catalyst also indicated the noticeable photo-catalytic degradation of MB, but about 72% of the MB (Figure S6e: Figure 8a; Panel B) was degraded after 50 min. Whereas, SWCO with singlet nanoplates as building blocks could degrade 60% of the MB (Figure S6d: Figure 8a; Panel D) within 50 min. In comparison the commercially available CuS powder under the same degradation conditions appeared to be much slower (Figure S6c, Figure 8a; Panel D).

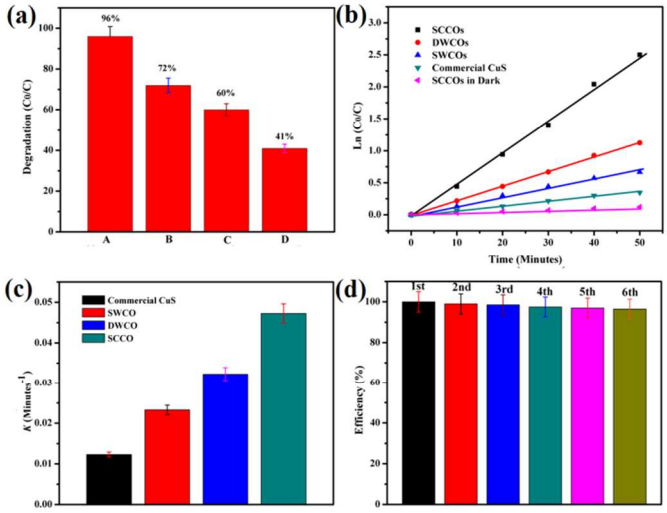

Figure 8 (a) A plot of the extent of photodegradation of MB aqueous solution by different catalysts (20mg) within 50Min of natural light irradiation at room temperature. Panel A: SCCO + H_2O_2, Panel B: SWCO + H_2O_2, Panel C: DWCO + H_2O_2, Panel D: Commercial CuS powder + H_2O_2, (b) The MB normalization concentration (from the optical absorbance measurements at 604nm) in the solution with different catalysts vs. the exposure time of the as prepared CuS products and commercially available CuS powder under different conditions, (c) First order rate constant K (min^{-1}) of the as prepared CuS products and commercially available CuS powder, (d) Stability test of as prepared CuS SCCO in degrading of MB aqueous solution for 6 repeated cycles.

The decomposition of the MB aqueous solution within 50min in the presence of the above as prepared samples and the commercial CuS powder is as follows: SCCO of CuS (96%) > DWCO of CuS (72%) > SWCO of CuS (60%) >CuS commercial powder (41%). Fig. 8b shows the curves of the concentration of residual MB with irradiation time. Without any catalyst, no decrease in the concentration of MB was detected under the natural light irradiation. The catalytic activity of the CuS architectures in the dark was also performed, which showed that only a little decrease in the concentration of MB was detected in the dark, which confirmed the concentration decrease of MB solution is mainly due to photodegradation of the products. The addition of catalysts lead to obvious degradation of MB, and the photocatalytic activity strongly depends on the morphology. CuS SCCO photo-catalyst demonstrated superiority, as visualized from the first order rate constant (K/min) of CuS SCCO (0.047247/min), CuS DWCO having doublet nanoplates building blocks (0.03229/min), CuS SWCO having singlet nanoplates building units (0.02329/min) and CuS commercial powder (0.012302/min) as shown in Figure 8c . First order rate constant is calculated by following equation.

$$\mathrm{Ln}(C_o/C) = kt \qquad (1)$$

Moreover, as a representative the as synthesized SCCO was recycled 6 times for degradation of MB to ascertain the stability; a significant recycling capability has been witnessed with only a very minor reduction in its activity (Figure 8d).

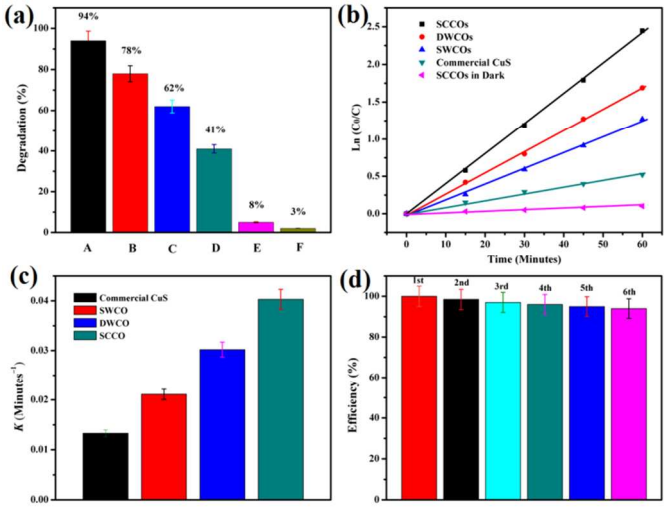

Figure 9 (a) A plot of the extent of photodegradation of RhB aqueous solution by different catalysts (20mg) within 60Min of natural light irradiation at room temperature. Panel A: SCCO + H_2O_2, Panel B: DWCO + H_2O_2, Panel C: SWCO + H_2O_2, Panel D: commercial CuS powder + H_2O_2, Panel E: Only SCCO in absence of H_2O_2, Panel F: Only H_2O_2 in the absence of any CuS catalyst. (b) The RhB normalization concentration (from the optical absorbance measurements at 553nm) in the solution with different catalysts vs. the exposure time of the as prepared CuS products and commercially available CuS powder under different conditions, (c) First order rate constant K (min^{-1}) of the as prepared CuS products and commercially available CuS powder, (d) Stability test of as prepared CuS SCCO in degrading of RhB aqueous solution for 6 repeated cycles.

Figure S7 shows the time- dependent absorption spectra of RhB aqueous solution containing as prepared SCCO, DWCO, SWCO and commercially available CuS powder as catalysts under the natural light irradiation in the presence of hydrogen peroxide. The characteristic absorption peak at 553nm of RhB was used as a monitored parameter during the photo-catalytic degradation process. The presence of only H_2O_2 without any catalyst and only SCCO as photo-catalyst in the absence of H_2O_2 contributed slightly within 60 min of irradiation (Figure S7a, b). The degradation of RhB aqueous solution in the presence of H_2O_2 and as prepared SCCO of CuS was observed to be 94% after 60min irradiation (Figure S7f; Figure 9a; Panel A) and maintained at a relatively stable level. Figure S6e shows the optical absorption spectra of RhB at different time intervals in the presence of as prepared DWCO, about 76% of the RhB (Figure 9a: Panel B) was degraded after 60min exposure time. Whereas, the as prepared SWCO with singlet nanoplates as building blocks could degrade only 60% of the RhB (Figure S7d, Figure 9a: Panel C) was degraded after 60 min. In comparison the CuS commercial powder could degrade the RhB 41% within the same irradiation time (Figure S7c, Figure 9a; Panel D). The degradation of the RhB aqueous solution within 60min in the presence of the above as CuS catalysts is as follows:

SCCO of CuS (94%) > DWCO of CuS (76%) > SWCO of CuS (62%) > CuS commercial powder (43%). Fig. 9b shows the curves of the concentration of residual RhB with irradiation time. The

catalytic activity of the CuS architectures in the dark showed only a little decrease in the concentration of RhB, which confirmed the concentration decrease of RhB solution is mainly due to photodegradation of the products. Moreover, the corresponding first order rate constant (K/min) of CuS SCCO (0.0403/min), CuS DWCO (0.0302/min), CuS SWCO (0.0211/min), CuS commercial powder (0.0133/min) are displayed in Figure 9b. Furthermore, the as synthesized SCCO showed a good recycling capability with a very minor reduction in its activity, as shown in Figure 9d.

In order to indicate a higher potential for practical applications, we applied the photo-degradation to mixed dyes aqueous solution. Since the industrial waste not only contains the singlet dye contamination it may comprise of mixture of dyes. This kind of catalyst can not only degrade single organic dyes, such as MB, RhB etc., but it also has an excellent ability in mixed solutions composed of different dyes. Guaranteeing that one dye in wastewater has been discharged in industry production is difficult if a kind of catalyst that can degrade several different dyes at the same time is used. The applied scope of such a catalyst must be improved significantly. To demonstrate the variety of degradation by the CuS products obtained, samples were applied to degrade a mixed solution of RhB and MB under similar conditions to that for MB and RhB separately. The changes in the UV-vis spectra during the removal of the mixed solution (MB + RB) by the as-obtained CuS hierarchical architectures are shown in Figure S8. Within the 56min of natural light irradiation the average removal of (MB+RhB) was found to be 93%, 72.5%, 61%, and 41% for SCCO, DWCO, SWCO and CuS Commercial powder, respectively (Figure 10c). Only H_2O_2 in the absence of CuS catalyst and the as prepared SCCO in the absence of H_2O_2 contributed none in the catalysis process, only 6% and 9% degradation of mixed dyes solution was witnessed, respectively (Figure 10a, b). Moreover, the as synthesized SCCO were recycled 6 times for degradation of mixed dyes solution (MB+RhB) with only a very minor reduction in its activity (Figure 10d).

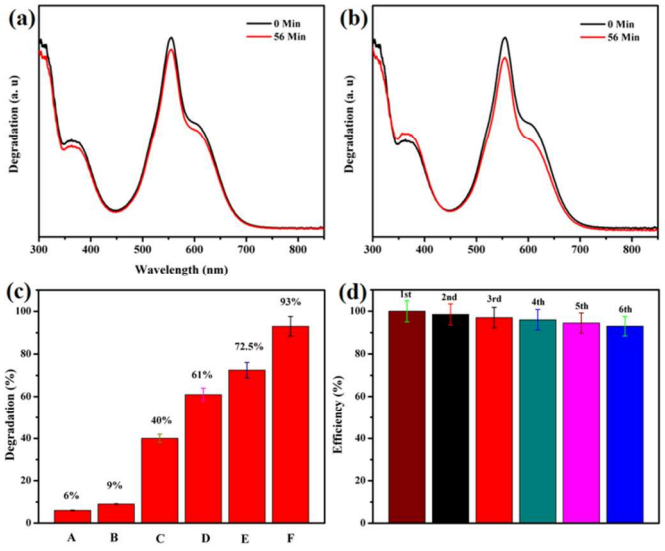

Figure 10 (a) Absorption spectra of photo degradation of mixed dyes (MB+RhB) solution under natural light by different catalysts (20mg) within 56Min of natural light irradiation at room temperature, (a) without any catalyst + H_2O_2, (b) SCCO + no H_2O_2, (c) A plot of the extent of photodegradation of mixed dyes (MB+RhB) aqueous solution by different catalysts. Panel A: Only H_2O_2, Panel B: SCCO + no H_2O_2, Panel C: commercial CuS powder + H_2O_2, Panel D: SWCO + H_2O_2, Panel E: DWCO + H_2O_2, Panel F: SCCO + H_2O_2, (b) Stability test of as prepared CuS SCCO in degrading mixed dyes aqueous solution for 6 repeated cycles.

Overall, the improvement in degradation rate of MB, RhB and their mixed aqueous solution relies on the synergistic effect of H_2O_2 and the as prepared CuS catalysts.[34-37] A brief description of the reaction mechanism in this degradation process is described below.

$$Cu^{2+} + H_2O_2 \longrightarrow H^+ + CuOOH^+ \quad (1)$$
$$CuOOH^+ \longrightarrow HOO^{\cdot} + Cu^+ \quad (2)$$
$$Cu^+ + H_2O_2 \longrightarrow Cu^{2+} + OH^- + HO^{\cdot} \quad (3)$$

$HO^{\cdot}$ radicals can attack on organic substrates MB, RhB and the mixture of organic dyes such as:

$$MR + HO^{\cdot} \longrightarrow MR^{\cdot} + H_2O \quad (4)$$

The highest photo-catalytic activity of CuS SCCO for enhanced degradation of MB, RhB, and the mixed dyes aqueous solution, among all the as prepared CuS products is due to several factors. Firstly, the SCCO have the largest surface area (41 $m^2\ g^{-1}$) due to their entire hierarchical existence with nanoplates building blocks and unique double pore sizes with mesopores existence. So, it is generally acceptable that the SCCO can provide more active catalytic sites for photo-catalytic reactions.[38] Secondly, the hierarchical SCCO due to a lot of unfolded and extremely enriched nanoplates possess plenty of pores within the hierarchically interconnected building units, which not only reduce reflection and harvest more light, can also contribute to the transport for the molecules of organic contaminants to get to the active sites on inner sides as well.[39] So the nanoplates could absorb more photons to produce electron–hole pairs under natural light, [38] and these deep and capacious pores enable the hierarchical structures to be exposed to the dye solution sufficiently. Furthermore, the nano-size of plates itself could reduce the radiationless recombination of electron–hole pairs, [39] which is also in favor of the enhanced photocatalysis of organic dyes aqueous solutions. Moreover, the better crystallinity of CuS SCCO and smaller crystallite size (38nm) (Figure S9) along with good dispersing and uniformity as compared to the as synthesizd DWCO and SWCO as well as is highly supportive in photocatalytic degradation of organic dyes.[39-41]

This structure in the form of SCCO is stable under any atmosphere environment; thus, catalysts with such structure can be maintained at a highly efficient catalytic level after several repeated catalytic reactions. Compared with Fe^{2+} in the Fenton method, this catalyst exhibits various advantages; this catalyst can be used repeatedly without bringing colored metal ions into the whole catalytic system, and can be used as a degrading catalyst in highly concentrated wastewater because of its low cost, simple operation, and highly efficient properties. Also this catalyst could be easily recycled, whereas Fenton catalysts cannot. Furthermore, the remaining Fe^{3+} in the Fenton catalyst could change the color of the whole reaction system. In particular, three-dimensional (3D) hierarchical architectures in the form of SCCO assembled by nanostructured building blocks have been well investigated for their improved properties originating from their building blocks. These distinguishing features are expected to be more advantageous than those of the powder samples, matching well with the principle of a highly efficient catalyst design.

Thus based on the above discussion; it is excellently believable that the photo-catalytic superiority of the as prepared CuS SCCO with hierarchically interconnected nanoplates as building blocks is attributed to their high specific surface area, wholly exposed and supereme hierarchical building blocks, good crystallinity, small crystallite size, excellent dispersing and uniformity. Since the photo degradation experiment of organic dyes was carried out under illumination by natural light, suggest the potential application might be quite feasible in practice.

Conclusions

In summary, a well-controlled synthesis of number of CuS complex and hierarchical morphologies fully exposed with nanoplates building blocks has been successfully achieved. The photo-catalytic superiority of CuS SCCO for degradation of highly concentrated dyes under natural light have been attributed to their considerable high surface area, isolated existence and entire hierarchical existence. The present study not only opens a new horizon for the synthesis of isolated, multi-complex and unusual morphologies based on nanoplates building blocks for many other chalcogenides, but also is of fundamental importance for the investigation of their potential applications in other fields, including sensors, optics, and so forth.

Acknowledgements

This work was supported by National Natural Science Foundation of China (21371023, 50972017) and the Research Fund for the Doctoral Program of Higher Education of China (20101101110026).

Notes and references

[1]Research Centre of Materials Science, Beijing Institute of Technology, Beijing 100081, P. R. China
[2]Department of Materials Science and Engineering, College of Engineering, Peking University Beijing 100871, China

1. C. Burda, X. B. Chen, R. Narayanan and M. A. El-Sayed, *Chem. Rev*., 2005, **105**, 1025. (b) F. K. Butt, C. Cao, W. S. Khan, M. Safdar, X. Fu, M. Tahir, F. Idrees, Z. Ali, G. Nabi and D. Yu, *CrystEngComm*, 2013,**15**, 2106.; (c) Y. Xuelian, C. Cao, H. Zhu, *Adv. Funct. Mater.*, 2007, **17**, 1397.; (d) X.L. Yu, Y. Wang, H.L.W. Chan, C. B. Cao, *Microporous and Mesoporous Materials*, 2009,**118**, 423.
2. S. H. Jiao, L. F. Xu, K. Jiang and D. S. Xu, Adv. Mater., 2006, **18**, 1174. (b) M. Tahir, C. Cao, F. K. Butt, F. Idrees, N. Mahmood, Z. Ali, I. Aslam, M. Tanveer, M. Rizwan and T. Mahmood, *J. Mater. Chem. A*, 2013, **1**, 13949; (c) M. Tahir, C. Cao, N. Mahmood, F. K. Butt, A. Mahmood, F. Idrees, S. Hussain, M. Tanveer, Z. Ali, I. Aslam, *ACS Appl. Mater. Interfaces* 2014, **6**, 1258.
3. W. X. Zhang, Z. X. Chen and Z. H. Yang, Phys. Chem. Chem. Phys., 2009, **11**, 6263. (b) F. Idrees, C. Cao, F. K. Butt, M. Tahir, M. Tanveer, I. Aslam, Z. Ali, T. Mahmood and J. Hou, CrystEngComm, 2013, **15**, 8146. (c) F. Idrees, C. Cao, F. K. Butt , M. Tahir, I. Shakir, M. Rizwan, I. Aslam, M. Tanveer, Z. Ali, Int. Journal of hyd. Energy, 2014, **39**, 13174
4. H. L. Cao, X. F. Qian, C. Wang, X. D. Ma, J. Yin and Z. K. Zhu, J. Am. Chem. Soc., 2005, **127**, 16024. (b) M. Tanveer, C. Cao, Z. Ali, I. Aslam, F. Idrees, W. S. Khan, F. K. Butt, M. Tahir and N. Mahmood, *CrystEngComm*, 2014, **16**, 5290.
5. Z. Y. Wang, D. Y. Luan, C. M. Li, F. B. Su, S. Madhavi, F. Y. C. Boey and X. W. Lou, *J. Am. Chem. Soc*., 2010, **132**, 16271.
6. Y. Qin, R. C. Che, C. Y. Liang, J. Zhang and Z. W. Wen, *J. Mater. Chem*., 2011, **21**, 3960.
7. H. G. Zhang, Q. S. Zhu, Y. Zhang, Y. Wang, L. Zhao and B. Yu, *Adv. Funct. Mater*., 2007, **17**, 2766.
8. F. Caruso, R. A. Caruso and H. Mohwald, Science, 1998, **282**, 1111.
9. S. J. Ding, J. S. Chen, G. G. Qi, X. N. Duan, Z. Y. Wang, E. P. Giannelis, L. A. Archer and X. W. Lou, *J. Am. Chem. Soc*., 2011, **133**, 21.
10. M. S. Yavuz, Y. Y. Cheng, J. Y. Chen, C. M. Cobley, Q. Zhang, M. Rycenga, J. W. Xie, C. Kim, K. H. Song, A. G. Schwartz, L. V. Wang and Y. N. Xia, *Nat. Mater*., 2009, **8**, 935.
11. Zhen Li, Liwei Mi,Weihua Chen, Hongwei Hou, Chuntai Liu, Hailei Wang, Zhi Zheng and Changyu Shenc, *CrystEngComm*, 2012, **14**, 3965.
12. K. V. Singh, A. A. M. Morales, G. T. S. Andavan, K. N. Bozhilov and M. Ozkan, *Chem. Mater*., 2007, **19**, 2446. (b) I. Aslam, C. Cao, M. Tanveer, W. S. Khan, M. Tahir, M. Abid, F. Idrees, F. K. Butt, Z. Ali and N. Mahmood, New J. Chem., 2014, **38**, 5462. (c) I. Aslam, C. Cao, W. S. Khan, M. Tanveer, M. Abid, F. Idrees, R. Riasat, M. Tahir, F. K. Butt and Z. Ali, RSC Adv., 2014, 4, 37914. (d) M. Tanveer, C. Cao, I. Aslam, Z. Ali, F. Idrees, W. S. Khan, F. K. Butt, M. Tahir and A. Mahmood, *Sci.of Adv. Mater.*, 2014, **6**, 1.

13 . X. W.Lou,C. Yuan,L. A. Archer, *Advanced Materials*, 2007, **19**, 3328.

14. Cheng, Zhiguo, Shaozhen Wang, Qian Wang and Baoyou Geng, CrystEngComm12 (2010):144-149.

15 . J. G. Yu, J. Zhang and S. Liu, *J. Phys. Chem*., 2010, **114**, 13642.
16 . Yu, J. G., Hai, Y., Cheng, B. *J. Phys. Chem. C*, 2011, **115**, 4953.
17. Ghijsen, J., Tjeng, L. H., Elp, J. V., Eskes, H.; Westerink, J., Sawatzky, G. A.; Czyzyk, M. T. *Phys. Rev. B*, 1988, **38**, 11322.
18. Todd, E. C., Sherman, D. M. Am. Mineral., 2003, **88**, 1652.
19. F. Li, J. F. Wu, Q. H. Qin, Z. Li and X. T. Huang, *Powder Technol*., 2010, **198**, 267**.**
20. Jixiang Fang, Bingjun Ding, and Xiaoping Song, *crystal growth & design* 2008, **8**, 3616.
21. Fievet, F., Lagier, J. P.; Blinb, B., Figlarz, M. *Solid State Ionics*, 1989, **32**, 198.
22. H. Colfen and M. Antonietti, *Angew. Chem*., Int. Ed., 2005, **44**, 5576.
23. H. Colfen and S. Mann, *Angew. Chem*., Int. Ed., 2003, **42**, 2350.
24. L. S. Zhong, J. S. Hu, H. P. Liang, A. M. Cao, W. G. Song and L. J. Wan, *Adv. Mater*., 2006, **18**, 2426.
25. Zhang, P. Gao, L. *J. Mater.Chem*., 2003, **13**, 2007.
26. Gao, J. Li, Q. Zhao, H. Li, L. Liu, C. Gong, Q. Qi, L. *Chem. Mater*., 2008, **20**, 6263.
27. Chen, L. Yu, W. Li, Y. *Powder Technology*, 2009, **52**, 191.
28. S. K. Haram, A. R. Mahadeshwar, S. G. Dixit, *J. Phys. Chem*., 1996, **100**, 5868.
29. A. M. Qin, Y. P. Fang, H. D. Ou, H. Q. Liu, C. Y. Su, *Cryst. Growth Des*., 2005**, 5**, 855.
30. S. M. Ou, Q. Xie, D. K. Ma, J. B. Liang, X. K. Hu, W. C. Yu, Y. T. Qian, *Mater. Chem. Phys*., 2005, **94**, 460.
31. K. P. Kalyanikutty,M. Nikhila, U. Maitra, C. N. R. Rao, *Chem. Phys. Lett*., 2006, **190**, 432.
32. J. Shi, J. Li, X. J. Huang and Y. W. Tan, *Nano Res.*, 2011, **4**, 488.
33. H. Xu, W. Wang and W. Zhu, *J. Phys. Chem. B*, 2006, **110**, 13829.
34. D. F. Ollis, E. Pelizzetti, N. Serpone, *Environ. Sci. Technol*., 1991, **25**, 1522.
35. T. Y. Wei, Y. Y. Wang, C. C. Wan, *J. Photochem. Photobiol*. A,, 1990, **55** 115.
36. J. L. Elechiguerra, J. R. Gasga and M. J. Yacaman, *J. Mater. Chem*., 2006, **16**, 3906.
37. Z. H. Wang, S. P. Zhao, S. Y. Zhu, Y. L. Sun and M. Fang, *CrystEngComm*. 2011, **13**, 2262.
38. L. Zhang, H. Yang, J. Yu, F. Shao, L. Li, F. Zhang, H. Zhao, *J. Phys. Chem. C*, 2009, **113**, 5434.
39. G. Tian, Y. Chen, W. Zhou, K. Pan, Y. Dong, C. Tian, H. Fu, *J. Mater. Chem*., (2010).
40. C. H. Ye, Y. Bando, G. Z. Shen and D. Golberg, *J. Phys. Chem. B*, 2006, **110**, 15146.
41. J. S. Hu, L. L. Ren, Y. G. Guo, H. P. Liang, A. M. Cao, L. J. Wan and C. L. Bai, *Angew. Chem*., Int. Ed., 2005, **44**, 1269.

